Original Article

Ring sign: an imaging sign for osteochondromyxoma in Carney complex

Wei Yu[1], Zai-Zhu Zhang[1], Ou Wang[2], Ming-Qian Huang[3], Wei-Bo Xia[2], Ali Guermazi[4]

[1]Department of Radiology, [2]Department of Endocrinology, Peking Union Medical College Hospital, Beijing 100730, China; [3]Department of Radiology, Stony brook University Hospital, Syosset, NY 11791, USA; [4]Department of Radiology, Boston University School of Medicine, Boston, MA 02118, USA

Correspondence to: Wei Yu, MD, PhD. Department of Radiology, Peking Union Medical College Hospital, Beijing 100730, China.
Email: weiyu5508@yahoo.com.

Background: To introduce the concept of "ring sign" and to evaluate its role in the diagnostic imaging of osteochondromyxoma in patients with Carney complex (CNC).

Methods: Three patients presenting osteochondromyxoma with CNC were included for evaluation of the ring sign on different imaging modalities, including radiographs, computed tomography, and magnetic resonance imaging. The literature was reviewed for further discussion.

Results: The ring sign in osteochondromyxoma could be seen on radiographs, computed tomography, and magnetic resonance images in all three patients at each of the involved sites. The morphological patterns and the number of ring signs varied by case, site, and imaging method. Some previous reports have shown images that contain ring signs, but do not identify them as such.

Conclusions: Ring sign can be considered as a relatively specific sign, helpful for the imaging diagnosis of osteochondromyxoma in the CNC.

Keywords: Carney complex (CNC); radiograph; computed tomography; magnetic resonance imaging; osteochondromyxoma; ring sign

Submitted Aug 22, 2019. Accepted for publication Nov 18, 2019.
doi: 10.21037/qims.2019.11.14
View this article at: http://dx.doi.org/10.21037/qims.2019.11.14

Introduction

In 1985, Carney *et al.* (1) first reported a rare, autosomal dominant hereditary complex characterized by myxomas, spotty skin pigmentation, and endocrine overactivity, which was then named Carney complex (CNC). Stratakis *et al.* (2) summarized the symptoms, signs, and family history of reported cases in 2001, and established the diagnostic criteria for CNC. The main diagnostic criteria are as follows: (I) spotty skin pigmentation with a typical distribution (lips, conjunctiva, and inner or outer canthi, vaginal and penile mucosa); (II) myxoma (cutaneous and mucosal); (III) cardiac myxoma; (IV) breast myxomatosis or findings on fat-suppressed magnetic resonance imaging suggestive of this diagnosis; (V) primary pigmented nodular adrenocortical disease (PPNAD) or paradoxical positive response of urinary glucocorticosteroids to dexamethasone administration during Liddle's test; (VI) acromegaly due to growth hormone (GH)-producing adenoma; (VII) large-cell calcifying Sertoli cell tumor (LCCSCT) or characteristic calcification on testicular ultrasonography; (VIII) thyroid carcinoma or multiple, hypoechoic nodules on thyroid ultrasonography, in a young patient; (IX) psammomatous melanotic schwannoma (PMS); (X) blue nevus or epithelioid blue nevus (multiple); (XI) breast ductal adenoma (multiple); (XII) osteochondromyxoma (OMX). OMX is one of the main diagnostic criteria, yet also one of the least common presentations of CNC (2).

First reported by Poli in 1955, OMX is a rare, chondrogenic, benign tumor (3). The tumor is one of the lesions in the CNC and is also known as the "Carney bone

tumor" (2). Given the extremely low prevalence of OMX in CNC [approximately 2% of CNC patients (2,4)], the reports on OMX images were preciously few. To our knowledge, no specific imaging sign has been reported for OMX in CNC, although a few reports have noted some of the imaging features. Therefore, we looked for the specific "ring sign" on radiographs, computed tomography (CT), and magnetic resonance imaging (MRI) of three OMX patients treated in our hospital, whom all met the diagnostic criteria of CNC (2).

Methods

Patient data

One male and two female patients (mean age, 27.3 years; range, 27–28 years) who presented to Peking Union Medical College Hospital, China, between June 2014 to December 2018, were included in the study. Informed consent from the patients was not required for this retrospective study as patient privacy was maintained. All three patients had typical skin pigmentation with a specific distribution (lips, conjunctiva and inner or outer canthi, vaginal and penile mucosa), endocrine overactivity, and bilateral adrenal nodular hyperplasia which were proven to be primary pigmented nodular adrenocortical disease (PPNAD) on postoperative pathology, and thus met the diagnostic criteria of CNC (2).

The sites of bone involvements in all three patients with OMX included the skull, spine, pelvis, femurs, tibiae, radii, and hands, as demonstrated by radiograph, CT, and MRI. Two patients had both radiographs and CT images for the skull, spine, and proximal femurs; all three patients had MRI for the skull; two patients had MRI for the spine and proximal femurs; one patient had radiographs for the distal left femur, left tibia, right radius, and bilateral hands.

Image analysis

Images for all bone abnormalities were analyzed by two radiologists for the following features: distribution, shape, density/intensity, enhancement, site, number, and size of lesions. For distribution, all bone lesions were classified into two types: (I) focal type, defined as solitary or multiple lesions that can be separated from one another; (II) diffuse type, defined as multifocal lesions that coalesce into diffuse lesions with no clear margins between them. The focal type was then categorized into three different patterns based on the shape: ring sign, irregular ring sign, and bubble sign. Ring sign does indeed look like a ring. For the ring sign, if the ring was not round, we designated it as an "irregular ring sign"; if the rings were aggregated, we defined it as a "bubble sign". For questionable cases, the consensus was reached with a joint reading by the two radiologists.

Results

Ring sign, irregular ring sign, and bubble sign were shown with different densities or signal intensities (SI) on radiographs, CT, and MRI (*Figures 1-7*). On radiographs and CT images, the margin of the ring presented as hyperdense while the center presented as hypodense (*Figure 1C,D*, *Figure 2A,B,C,D,E,F*, *Figure 4C,D*, *Figure 5A,B,C,D,E,F,G,H*, arrow). The margin was composed of low SI areas, or of high SI areas on T1- and T2-weighted MRI; the center had low or slightly equal SI (compared with the SI of muscle) on the T1-weighted MRI and high or low SI on the T2-weighted MRI (*Figure 1E,F,G,H,I*, *Figure 3C,D*, *Figure 4E,F,G,H*, arrow). The centers of the ring signs were markedly and heterogeneously enhanced on contrast-enhanced TI-weighted MRI (*Figure 3F*, *Figure 4H*, *Figure 6H*, *Figure 7D*).

Focal type

Ring signs were shown on radiographs in one patient with two sites [distal left femur (n=1) and proximal left tibia (n=1)], CT images in two patients with four sites [spine (n=2), pelvis (n=2)], and MRI in only one patient with one site [spine (n=1)]. More ring signs were revealed on CT and MRI than on radiographs. Especially for sites of the spine and pelvis, all rings which were found on both CT and MRI were not shown on the radiographs (*Figure 1A,B*, *Figure 4A,B*). Also, as shown in *Table 1*, 7 (30%) rings were detected by radiographs, 62 (77%) by CT, and 30 (81%) by MRI. The ring size was different on radiographs, CT, and MRI. The diameters for rings ranged from 0.5 to 1.0 cm on radiographs, 0.3 to 1.1 cm on CT, and 0.3 to 0.9 cm on MRI.

Irregular ring signs were seen on radiographs in two patients with five sites [proximal bilateral femur (n=2), distal left femur (n=1), proximal left tibia (n=1), and left fourth proximal phalanx (n=1)], CT images in two patients with four sites [spine (n=1), pelvis (n=1), and proximal bilateral femur (n=2)], and MRI in only one patient with one site [spine (n=1)]. As shown in *Table 1*, 7 (30%) irregular rings were detected by radiographs, 10 (12%) by CT, and three (8%) by MRI. The maximum diameters of irregular rings ranged from 1.0 to 2.7 cm on radiographs, 0.8 to 2.8 cm on CT, and 0.8 to 1.5 cm on MRI.

Figure 1 A 27-year-old female patient with multiple bones involved. (A) The posteroanterior (PA) and (B) lateral (LAT) spine radiographs showed no obvious abnormalities. (C) Sagittal and (D) axial computed tomography (CT) showed multiple ring signs or irregular ring signs (arrow). (E) Sagittal T1-weighted magnetic resonance imaging (MRI), (F) sagittal T2-weighted MRI, and (G) fat-suppressed T2-weighted MRI of the spine showed multiple ring signs or irregular ring signs (arrow). The ring sclerotic regions shown on CT were low SI on (H) T1-weighted MRI and (I) fat-suppressed T2-weighted MRI, while the center of these lesions which were hypodense on CT images were low SI on (H) T1-weighted images and high SI on (I) fat-suppressed T2-weighted MRI (arrow).

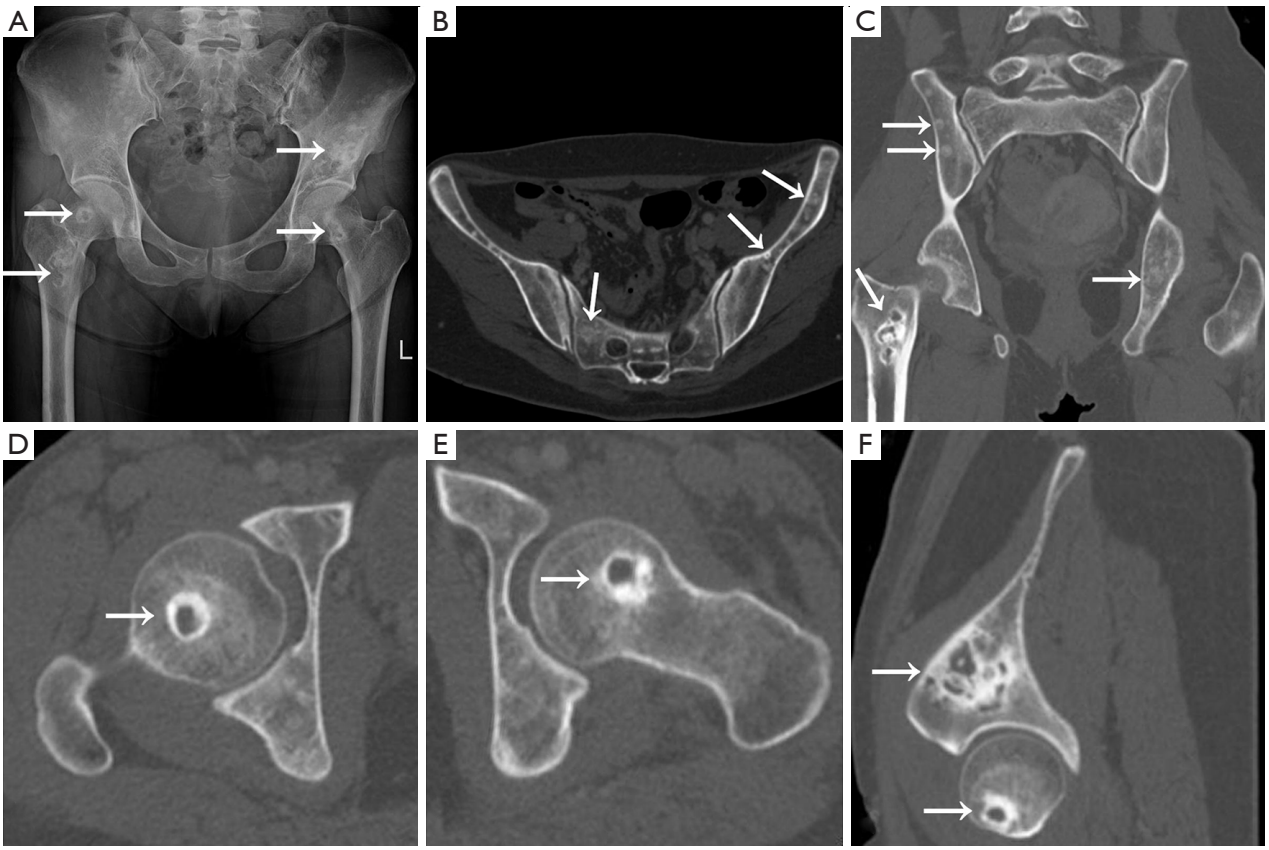

Figure 2 The same patient as in *Figure 1*. (A) Posteroanterior (PA) radiograph, (B) axial, (C) coronal, (D,E) axial, and (F) sagittal computed tomography (CT) of the pelvis and bilateral femurs showed multiple and varied-size ring signs, irregular ring signs, and bubble signs in the pelvis and bilateral femurs (arrow).

Bubble signs were shown on radiographs in two patients with eight sites [pelvis (n=1), proximal bilateral femur (n=2), middle left tibia (n=1), proximal right radius (n=1), left second distal metacarpal (n=1), right second proximal phalange (n=1), and right second proximal metacarpal bone (n=1)], CT images in two patients with 5 sites [spine (n=1), pelvis (n=2), and proximal bilateral femur (n=2)], and MRI images in only one patient with one site [spine (n=1)]. As shown in *Table 1*, 9 (40%) bubbles were detected by radiographs, 9 (11%) bubbles were detected by CT, and 4 (11%) bubbles were detected by MRI. The maximum diameters of bubbles ranged from 3.3 to 6.3 cm on radiographs, 1.2 to 5.1 cm on CT, and 1.1 to 2.2 cm on MRI.

Diffuse type

The diffuse type was only located on the skull, with the most common involved sites being the sinus and nasal bones. However, other craniofacial areas can be involved, including the frontal, temporal, zygomatic, occipital, and sellar regions. On radiographs, the lesions appeared as diffuse sclerotic thickening of the skull base with heterogeneous density with ill-defined margins, in which multiple irregular lytic lesions or bubble signs could be seen (*Figure 3A,B*, *Figure 6A,B*). On CT, the diffuse, ill-circumscribed, sclerotic, and lytic lesions could be distinguished clearly in the frontal, temporal, zygomatic, occipital, and sinus areas, as well as the sellar region (*Figure 6C,D*, *Figure 7A*). On MRI, the lesions were of mixed signal intensity on T1- and T2-weighted images with remarkable heterogeneous enhancement (*Figure 3C,D,E,F*, *Figure 6E,F,G,H*, and *Figure 7B,C,D*).

Discussion

It is well-known that imaging analysis can play an important

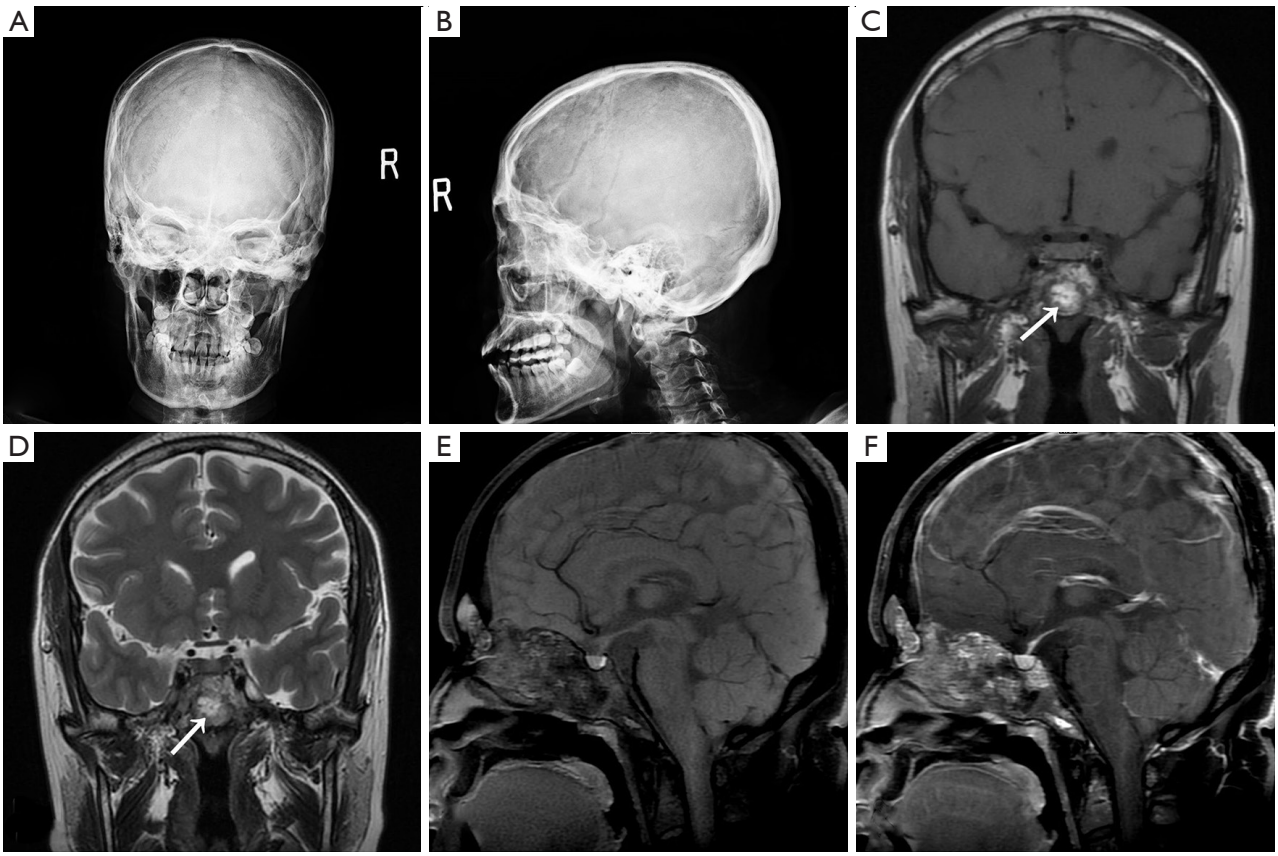

Figure 3 The same patient as in *Figure 1*. (A) Posteroanterior (PA) and (B) lateral (LAT) radiographs of the skull showed diffuse, sclerotic changes at the skull base; (C) Coronal T1-weighted magnetic resonance imaging (MRI), (D) coronal T2-weighted MRI, and (E) sagittal T1-weighted MRI showed bone lesions with mixed SI and ill-defined margins, in which ring signs appeared on T1- and T2-weighted MRI (C,D, arrow); (F) sagittal contrast-enhanced T1-weighted MRI showed remarkable and heterogeneous enhancement.

role in any diagnosis of a bone tumor. Different modalities provide different kinds of information, which may be helpful in understanding pathologic changes. OMX or "Carney bone tumor", is one of the diagnostic indexes for the CNC (5,6), even though its prevalence is low in CNC (2,4). Although various imaging findings have been reported (2,4-7), there is no deep knowledge about the role of different imaging modalities in the diagnosis of OMX in CNC, nor the specific imaging features they disclose.

We found examples of the ring sign in our study, but their pathological basis is unclear. Imaging demonstrated the margin of the ring signs was hyperdense on both X-ray and CT scans while being low SI on both T1- and T2-weighted MRI. Based on these findings, we speculate that the pathological basis of the ring margin may be caused by sclerotic bone or fibrous tissue. The center of the ring sign showed low density on X-ray and CT scans, while being mixed SI on T1- and T2-weighted MRI, indicating that unique cystic fluid cannot explain the center of the ring sign, especially when the central enhancement was found on contract-enhanced MRI (*Figure 3F*, *Figure 4H*, *Figure 6H*, and *Figure 7D*). Based on X-ray, CT, MRI, and contrast-enhanced MRI features, we speculate that granulation tissues with sufficient blood supply might be responsible for the pathology of the central region. On the other hand, we could not disclose the pathological basis for some ring margins with high SI areas on T1- and T2-weighted MRI. Therefore, future studies comparing imaging and pathology findings may shed light on the pathophysiology basis of the ring sign with different SI on imaging.

Ring signs, irregular ring signs, and bubble signs were found at different sites on the radiographs, CT and MRI in the three presented cases. For the ring sign, our results show that more ring signs have been revealed on CT and

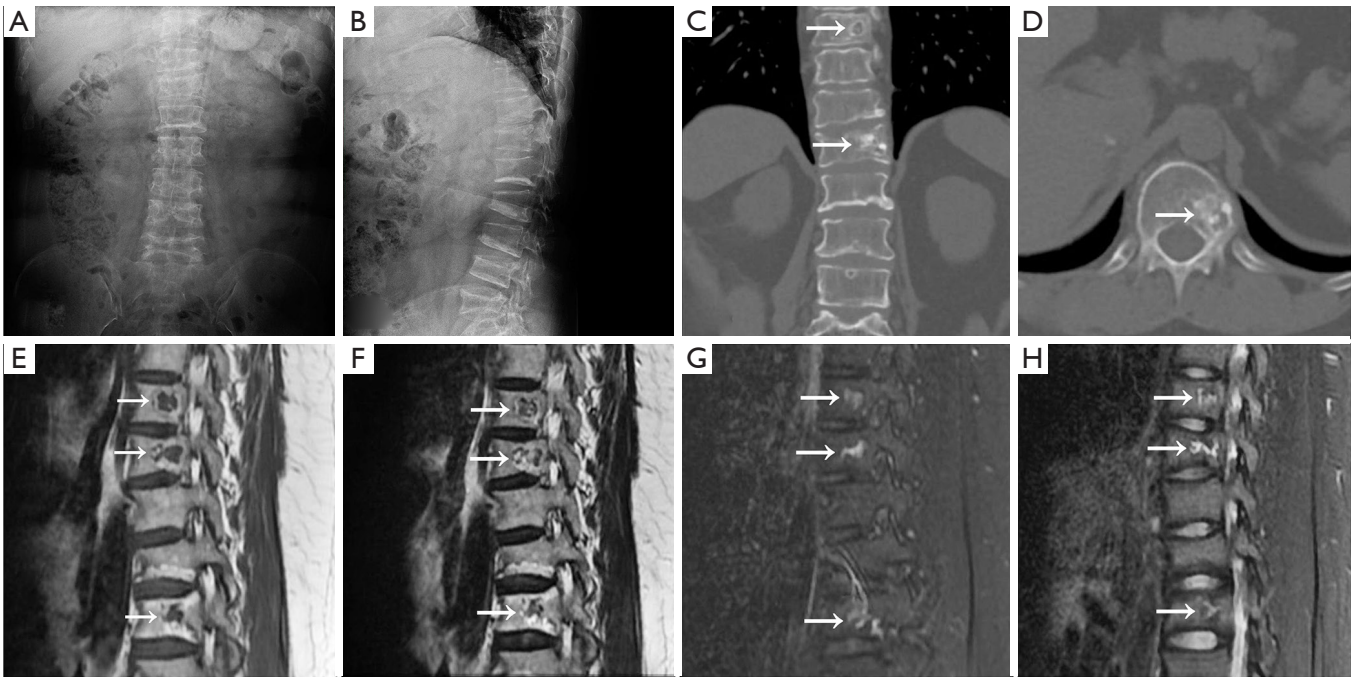

Figure 4 A 28-year-old female patient with multiple bones involved. (A) The posteroanterior (PA) and (B) lateral (LAT) spine radiographs showed that multiple vertebral bodies were flattened and wedge-shaped. (C) Reconstructed coronal and (D) axial CT showed that some vertebral bodies had multiple destructive lesions, presenting as multiple ring signs and bubble signs (arrow); (E) Sagittal T1-weighted, (F) sagittal T2-weighted, and (G) sagittal fat-suppressed T2-weighted magnetic resonance imaging (MRI) of the spine showed that multiple bubble signs appeared in some vertebral bodies (arrow). (H) Sagittal contrast-enhanced TI-weighted MRI showed that the centers of the bubble signs were markedly and heterogeneously enhanced (arrow).

MRI rather than on radiographs. Especially in the spine and pelvis, all rings found on both CT and MRI were not shown on radiographs. This is consistent with previous reported cases, as seen in Figure 2 in Carney *et al.* (5). This can be explained by the fact that the spatial resolution of both CT and MRI is higher than that of X-ray. Therefore, CT and MRI could reveal small ring signs which were hidden on radiographs. For the irregular ring and bubble signs, however, the results are different from that of the ring sign. This may be explained by the fewer numbers of both irregular and bubble lesions. Another explanation is that larger lesions for both irregular ring and bubble signs could not be hidden on radiographs, and could be easily shown on either X-ray, CT, or MRI scans. Therefore, we conclude that not only are ring signs, irregular ring signs, and bubble signs important to the imaging diagnosis but also that CT and MRI are more sensitive than X-ray in displaying the ring sign. CT and MRI also showed more abnormalities than X-ray suggesting both examinations may be helpful when radiographs alone cannot make the diagnosis.

Ring sign was seen on the coronal skull MRI (Figure 2A) in Waissbluth *et al.* (4) and on the sagittal spine T2-weighted and contrast-enhanced MRI (Figure 22A,B) in Courcoutsakis *et al.* (7). Nevertheless, neither author made any mention of the ring sign or a similar imaging feature. Therefore, we suggest that a lack of awareness of the ring sign may be the primary reason the disease has been considered to exhibit no specific imaging features in the literature (2,4-7).

Some limitations of this study should be addressed. First, the OMX lesions were not biopsied, although the definite diagnosis of CNC suggests OMX in the three cases. Moreover, the clinical findings and some of the imaging findings in cases 2 and 3 have been reported elsewhere (8). In fact, it is difficult and often unproductive to compare imaging findings directly with the larger, whole specimens taken from patients in clinical practice. The analysis above focuses on either using the imaging findings to explain the pathological changes or on using the pathological changes to understand abnormal imaging findings. This is similar to the previous analysis with MRI reported by Courcoutsakis *et al.* (7), which also lacked biopsy findings. In addition, due to the relatively

Figure 5 The same patient as in *Figure 4*. (A) Posteroanterior (PA) radiograph of the pelvis showed bubble signs in the proximal right femur (arrow); (B) PA and (C) lateral (LAT) radiographs of the left knee joint showed multiple ring signs and irregular ring signs at the distal femur and proximal tibia (arrow); (D) PA and (E) LAT radiographs of the left tibia and fibula showed a bubble sign in the middle tibia (arrow); (F) PA radiograph of the two hands showed bubble signs in the left second distal metacarpal, the right second proximal phalange and the right second proximal metacarpal bones (arrow); (G) PA and (H) LAT radiographs of the two forearms showed a bubble sign in the proximal right radius (arrow).

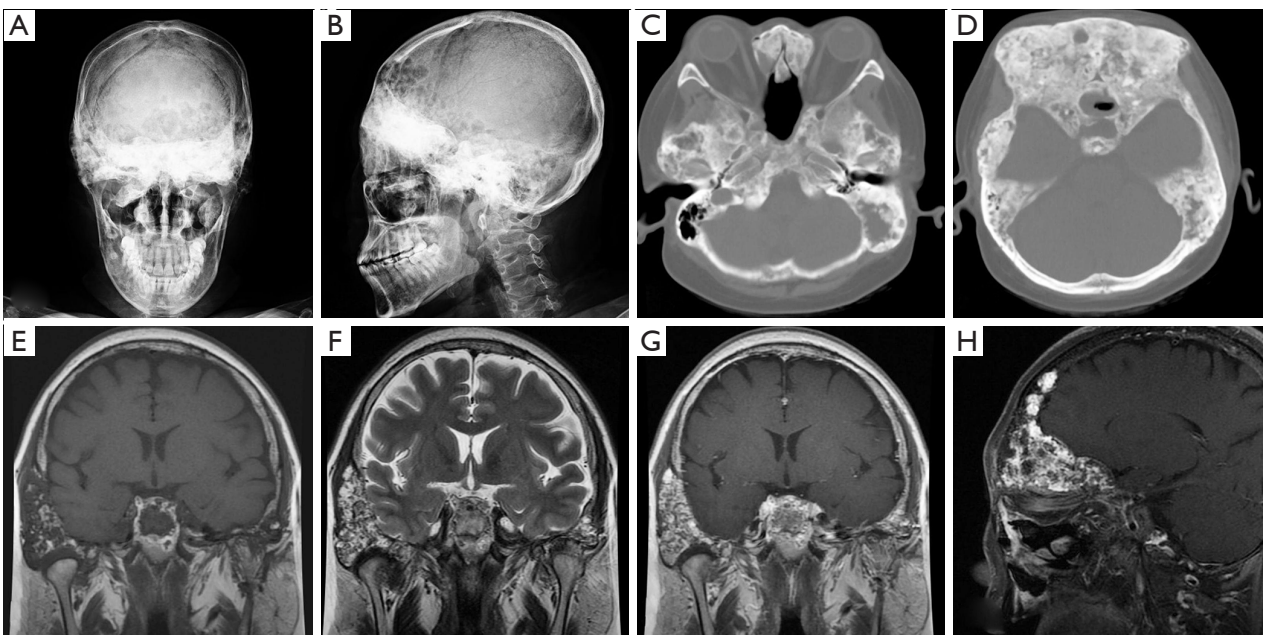

Figure 6 The same patient as in *Figure 4*. (A) The posteroanterior (PA) and (B) lateral (LAT) skull radiographs showed diffuse, sclerotic changes at the skull base. Multiple, irregular lytic lesions were seen in the frontal and temporal bones; (C,D) axial computed tomography (CT) of the skull showed multiple, diffuse sclerotic, and lytic lesions at the frontal, temporal, zygomatic, occipital, and sinus areas, as well as the sellar region; (E) coronal T1-weighted; (F) coronal T2-weighted; (G) coronal contrast-enhanced T1-weighted; and (H) sagittal contrast-enhanced T1-weighted MRI of the skull showed mixed signal intensity with remarkable enhancement.

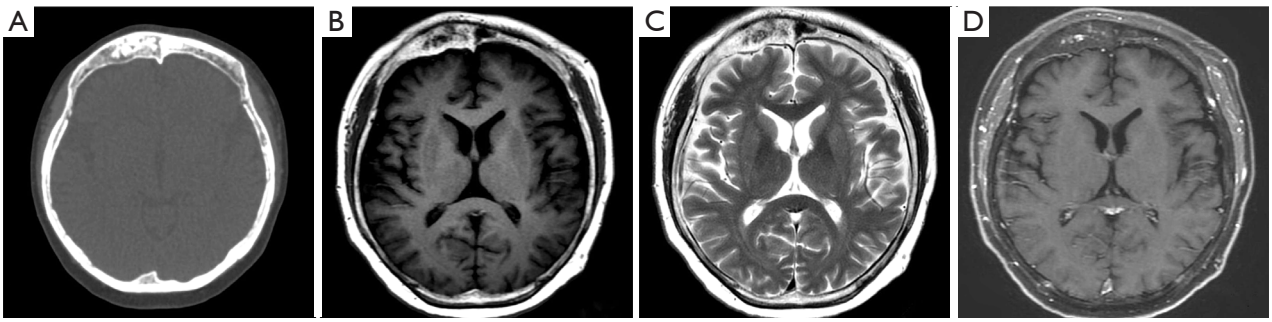

Figure 7 A 27-year-old male with Carney complex (CNC) involving the skull bones. (A) Axial computed tomography (CT) of the skull showed multiple, diffuse sclerosis and lucency in the cranial plate, which were markedly notable at the frontal bone; (B) axial T1-weighted; (C) axial T2-weighted; (D) axial contrast-enhanced TI-weighted MRI of the skull showed that the above bone lesions on CT were mixed signal intensities (SI) with remarkable and heterogeneous enhancement at the centers of bubble signs.

Table 1 Numeric results of focal type with different ring sign shown on three imaging modalities for all sites involved

Imaging modalities	Ring sign	Irregular ring sign	Bubble sign	Total
Radiographs	7 (30%)	7 (30%)	9 (40%)	23 (100%)
CT	62 (77%)	10 (12%)	9 (11%)	81 (100%)
MRI	30 (81%)	3 (8%)	4 (11%)	37 (100%)

small number of cases in our report and the previous references, statistical calculations about the prevalence of the ring sign could not be performed. They will, of course, be necessary in future analyses of a large sample of cases.

Based on the evidence presented in this study, we suggest that ring sign can contribute to the imaging diagnosis and differential diagnosis of OMX in CNC.

Acknowledgments

None.

Footnote

Conflicts of Interest: The authors have no conflicts of interest to declare.

References

1. Carney JA, Gordon H, Carpenter PC, Shenoy BV, Go VL. The complex of myxomas, spotty pigmentation, and endocrine overactivity. Medicine (Baltimore) 1985;64:270-83.
2. Stratakis CA, Kirschner LS, Carney JA. Clinical and molecular features of the Carney complex: diagnostic criteria and recommendations for patient evaluation. J Clin Endocrinol Metab 2001;86:4041-6.
3. Doyle LA. Sarcoma classification: an update based on the 2013 World Health Organization Classification of Tumors of Soft Tissue and Bone. Cancer 2014;120:1763-74.
4. Waissbluth S, Winter M, Dreyse X, Solar A, Castro M, Rosenblut A. Osteochondromyxoma of the nasal cavity: Case report and review of the literature. EJMCR 2018;2:12-5.
5. Carney JA, Boccon-Gibod L, Jarka DE, Tanaka Y, Swee RG, Unni KK, Stratakis CA. Osteochondromyxoma of bone: a congenital tumor associated with lentigines and other unusual disorders. Am J Surg Pathol 2001;25:164-76.
6. Golden T, Siordia JA. Osteochondromyxoma: Review of a rare carney complex criterion. J Bone Oncol 2016;5:194-7.
7. Courcoutsakis NA, Tatsi C, Patronas NJ, Lee CC, Prassopoulos PK, Stratakis CA. The complex of myxomas, spotty skin pigmentation and endocrine overactivity (Carney complex): imaging findings with clinical and pathological correlation. Insights Imaging 2013;4:119-33.
8. Li S, Duan L, Wang FD, Lu L, Jin ZY. Carney complex: two case reports and review of literature. World J Clin Cases 2018;6:800-6.

Cite this article as: Yu W, Zhang ZZ, Wang O, Huang MQ, Xia WB, Guermazi A. Ring sign: an imaging sign for osteochondromyxoma in Carney complex. Quant Imaging Med Surg 2019;9(12):1958-1965. doi: 10.21037/qims.2019.11.14

